Pose Optimization for Force and Stiffness Control of a redundant Robort Arm

Jieming Chen, Shizeng Zhang and Min Wu

Abstract— **Human beings predominantly use arm configurations to control the stiffness of our arms. For robot arms, a classical tool, used to describe the desired force/displacement behaviour at the end-effector, is the stiffness ellipsoid, whose geometry is affected by the stiffness matrix. This tool does not consider joint torque limit. Impedance control techniques set gains to realize the desired Cartesian feasibility region at the end-effector, so that robot configuration selection could appear secondary.**

In order to understand this discrepancy between human beings and robot arms, we investigate the ability of maintaining stiffness at the end-effector among different poses, and provide a series of analysis of the task-space force/displacement behaviour of non-redundant and redundant arms to illustrate why arm geometry plays a dominant role in robot interaction control. In this paper, we introduce the definition and physical meanings of SFR(stiffness feasibility regions),SFP(stiffness feasibility polytope) and SFE(stiffness feasibility ellipsoid). At last, we introduce the optimizations for the SFE, which includes two parts, optimizing the SFE geometry and minimizing the gravity effect on SFR translation and geometry.

I. INTRODUCTION

The task space capabilities of a manipulator to perform motion and/or to exert forces are of fundamental importance in robotics. In the design phase, their evaluation can be useful to determine the structure and the size of a manipulator that best fits the designer?s requirements. In the operational phase, they can be used to find a better configuration or a better operation point for a manipulator to perform a given task. When the end-effector interacts with the environment, forces are generated. In some specific cases, the end-effector of the robort needs to maintain the stiffness. For example, when the robort arm transport goods, the end-point is requored to maintain the stiffness so that the goods will not fall.

The idea of measuring the manipulating abilityof a robotic mechansim was first introduced in Yoshikawa where two ellipsoids, the (velocity) manipulability ellipsoid and the manipulating force ellipsoid, were defined. A dynamic manipulability ellipsoid was also introduced in Yoshikawa to characterize the achievable end-effector acceleration; in Chiacchio et al. A new definition of this ellipsoid was given to correctly take into account the contribution of gravity. The ellipsoids were revisited in Chiu, where they were used to measure the compatibility of manipulator configurations with a given task.

Impedence control is a robort interaction control. Its basic idea is to use the position deviation between the real position and the desired position to control the force the force of the end-effector.

$$\underline{M_d}\ddot{\underline{\delta x}} + \underline{K_d}\dot{\delta x} + \underline{K_p}\underline{\delta x} = \underline{F_a} \tag{1}$$

Here, equation (1) is the dynamic equation, $\underline{M_d}$ is the mass matrix, $\underline{K_d}$ is the damping matrix and $\underline{K_p}$ is the stiffness matrix, $\underline{F_a}$ is the force of the end-effector.

The stiffness matrix $\underline{K_p}$ is the connection between the force and the displacement. Without considerations of joint configurations and torque limits, any endpoint stiffness matrix can be realized in any arbitrary robot configuration[1]. To achieve an desired end-effector force, the stiffness matrix can be designed by the indirect force controller based on the relationship between the force and the displacement.

$$\underline{F_a} = \underline{K_p}\underline{\delta x} \tag{2}$$

with $\underline{K_p}$ denoting the stiffness matrix. Furthermore, when taking the torque limits and joint configurations into the consideration, the above equation (2) is not accurate because it does not consider the influence of the pose changes.

$$\underline{\tau} = \underline{J^T}\underline{F_a} \tag{3}$$

$$\underline{\tau} = \underline{J^T}\underline{K_p}\underline{\delta x} \tag{4}$$

The desired endpoint force/displacement are usually mapped to the joint-space mathematically, which is based on the jacobian matrix. The jacobian matrix is a velocity mapping from the work space to the joint space. This relationship can be translated to the (3). Based on equation (2) and (3), equation (4) can be calculated, which implies that the $\underline{\tau}$ inflects the stiffness.[2].[3].

Several studies measured the arm stiffness resulting from small hand displacement in stationary and dynamic conditions [4].[5]. underlying the body capabilities of restoring a desired configuration after being subjected to external perturbation. Stiffness is a measure of arm stability against noise and perturbation and its modulation has been studied during the execution of multijoint tasks requiring accuracy.[6].[7].

The stiffness ellipsoid is defined as the locus of the forces obtained $||F||$, corresponding to a deformation of unit norm, as depicted in Fig.1 The calculation of the stiffness ellipsoid is based on the SVD(singular value decomposition) of the stiffness matrix $\underline{K_p}$. The physical meaning of the stiffness ellipsoid is that how much force dose the operater need to push the end-effector for one meter.

The calculation of the stiffness ellipsoid is based on the equation (2), here, the joint configurations and the torque limits are not taken into considerations.

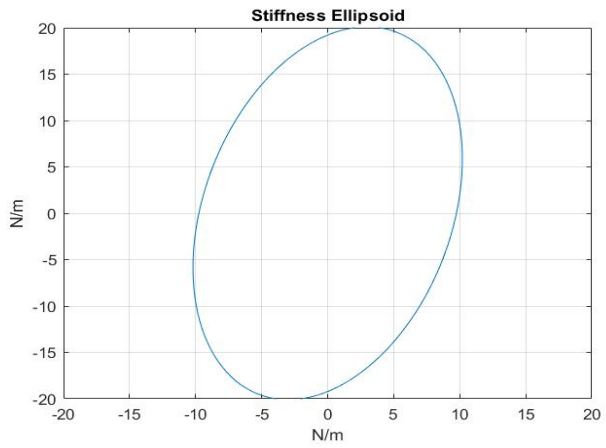

Fig. 1. Stiffness Ellipsoid

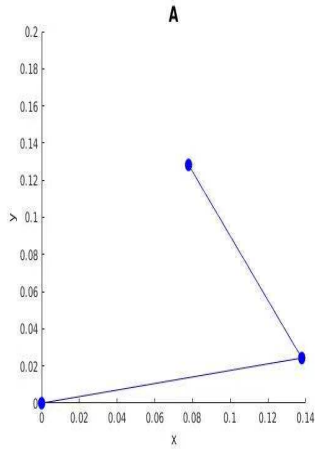

Fig. 2. configuration A

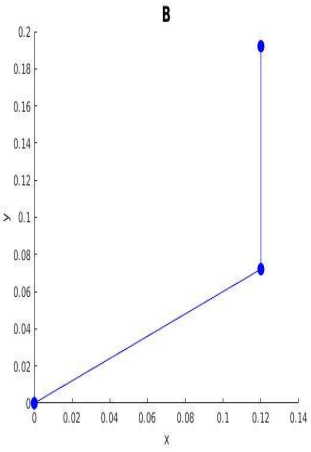

Fig. 3. configuration B

II. Interaction Boundaries of the Cartesian Force and Stiffness Control–NONREDUNDANT CASE

In reality, manipulators have boundaries, namely, torque limitations for every joint action. That means the e-e of the robot may fail to maintain the desired stiffness due to the torque limitations. As a result, we need to research the influence of the torque limitations on the manipulator performance. In order to indicate and research this influence specifically, we try to find the relationships between the e-e displacement and the torque of each joint under torque limitations. Furthermore, we transform this relationship from joint space into operational space which will be indicated later.

Let's consider a two-link manipulator in configuration A and configuration B as depicted in Fig.2 and Fig.3. Assume that the aim is to realize a desired stiffness matrix $K_{cd} = \begin{bmatrix} 1 & 0.2 \\ 0.2 & 2 \end{bmatrix}$ kN/m at the endpoint. For parameters, $q_A = [10°, 110°]$, L1 = 0.14 m, L2 = 0.12 m, $|\tau_1| \leq 3$ Nm and $|\tau_2| \leq 2$ Nm. The mass (m) of each link is assumed to be a point mass and located at the centre of mass of each link with m_1 = 4 Kg and m_2 = 2 Kg. For configuration B, it is the same manipulator as configuration A with $q_B = [31°, 59°]$ and it exposes to a similar external displacement profile.

Here, the aim is to investigate the relationship between e-e displacement and the torque of each joint. Consider that we have 360 directions and each direction has 0.25m moving horizon for e-e displacement. For each direction, dividing the moving horizon into 100 equal unit(0.0025m). Ideally, if not considering the influence of the torque limitations, the desired Force can be calculated based on (2). The configuration has changed due to the displacement of the e-e, as a result, the $\underline{J}$ needs to be calculated again. The calculation of the joint variable is based on the (5).

$$\underline{\dot{\delta x}} = \underline{J}\,\underline{\dot{\delta q}} \tag{5}$$

After that, the desired torque can be calculated based on the relationship between the joint torque and the force of the end effector, as shown in (6).

$$\underline{\tau_{des}} = \underline{J^T}\,\underline{F_{des}} \tag{6}$$

After applying the joint torque limits to the desired torque $\underline{\tau_{des}}$, the real torque $\underline{\tau_{real}}$ can be calculated. Till now, the relationship between the e-e displacement and the torque of each joint is available which is indicated in Fig.4 (upper plot). For calculating the relationship between the e-e displacement and the real force $\underline{F_{real}}$, we can use (7). The result is shown in Fig.4 (lower plot).

$$\underline{F_{real}} = \underline{(J^T)^{-1}}\,\underline{\tau_{real}} \tag{7}$$

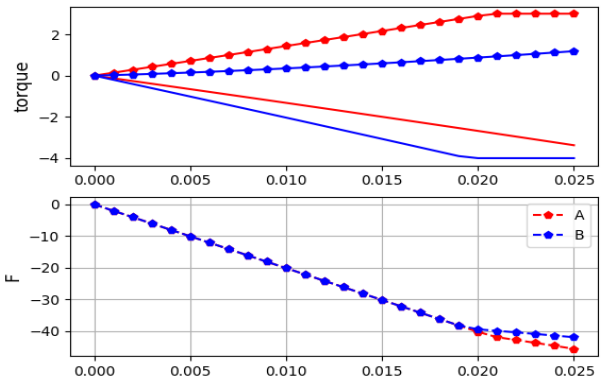

Fig. 4. joint torques versus displacements along $-y$-direction in manipulators A and B (upper plot), and the corresponding endpoint forces (lower plot).

As shown in Fig.4, the plot indicates that, for the same link of different configurations, the ability to maintain stiffness are different although they are under the same torque limitation. In conclusion, when we apply a Cartesian stiffness controller in a torque controlled robot to achieve a desired stiffness matrix, in a particular configuration, this is associated with a maximum allowable displacement region.

A. SFR(stiffness feasibility regions),SFP(stiffness feasibility polytope) and SFE(stiffness feasibility ellipsoid)

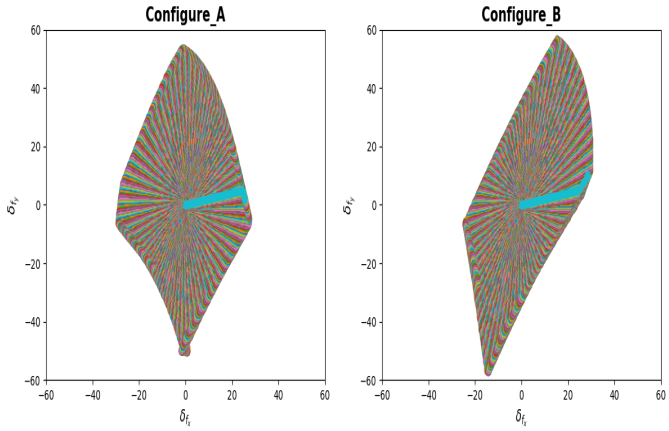

Fig. 5. locus of $\| F \|$

The force ellipsoid (shown in Fig.5) is defined as the locus of the force obtained $\| F \|$, corresponding to a deformation of unit norm. It is different from the stiffness ellipsoid which we mentained before. The method to get the stiffness ellipsoid is based on (2) without any limitation. However, the method to calculate the force ellipsoid is connected with the jacobi matrix and it considers about the torque limits.

It is important to note that the force locus in Fig.5 only conveys a "local" picture of the operational stiffness. If large displacement are applied at the end effector, it will get out of the feasibility boundaries, which means, under this specific direction, the end effector cannot maintain the stiffness any more. In addition, the translational effect of gravity, which varies due to the change in robot configuration, will contribute to the modifications in the geometry of such a boundary region [8]. This is generally an undesired effect since it will influence symmetric properties of the SFR with respect to the initial equilibrium point. These are the external influence that may affect the displacemnet of the e-e.

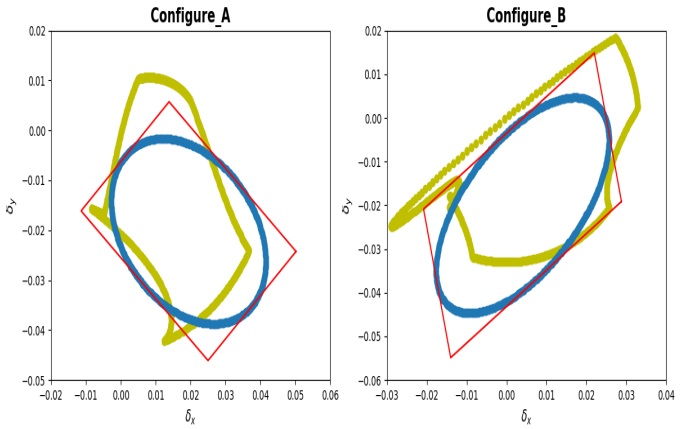

Fig. 6. Yellow plots illustrate the SFRs for configuration A (left) and B (right), while corresponding polytopes are plotted in red. SFEs are plotted in blue, for both configurations. The units are in meters [m].

SFR(stiffness feasibility regions) is defined as a maximum and real-time allowable boundary in the space of Cartesian displacement for e-e movement. The connection between the force ellipsoid and the SFR is that, the force ellipsoid denotes to the real force that the endpoint can realize and the SFR denotes to the maximum and real-time allowable displacement for the endpoint. This connection also supplys a basic idea for calculating the SFR.

For the SFR calculation, we use a similar method as we calculate the relationship between the e-e displacement and the force that the e-e can realize. Specifically, we use a progressive method to calculate the relationship between and real torque. After translating this relationship from joint space into operational space, we get the relationship between displacement and real force. Finally, based on (2), we can calculate the maximum allowable stiffness feasibility regions (SFR). The SFRs for the two-link example in configuration A (left plots) and B (right plots) are illustrated in Fig.6 in yellow. The basic idea of the SFR algorithm is indicated below.

Algorithm 1 GET SFR

output: The maximum range for maintaining stiffness, SFR;

$step\_length \leftarrow 0.001$;
for direction in 0-360 degree **do**
  Initialize the robot arm;
  while counter $<$ iter_num **do**
    $\underline{distance} \leftarrow counter * step\_length$;
    $\underline{F_{ext}} \leftarrow FORCEBYDISTANCE(\underline{distance})$;
    Update joint variables;
    Update e-e position;
    Update Jacobian Matrix;
    if joint torques reach torque limitations **then**
      SFR $\leftarrow \underline{distance}$;
      Break;
    end if
  end while
end for
function FORCEBYDISTANCE($\underline{distance}$)
  Calculate torque of gravity($\underline{\tau_g}$);
  $\underline{F\_ext} \leftarrow \underline{K_c} \cdot \underline{distance}$;
  $\underline{\tau} \leftarrow \underline{J(q)}^T \underline{F_{ext}} + \underline{\tau_g}$;
  $\underline{\tau}$ then is clipped by $\underline{\tau}$ limitations;
  $\underline{F_{res}} \leftarrow \underline{J^T(q)}^{-1} \underline{\tau} - \underline{\tau_g}$;
  Return $\underline{F_{res}}$;
end function

SFP(stiffness feasibility polytope) takes less time to calculate the feasibility region. The basic idea to calculate SFP is to project the force polytope of manipulator in a certain configuration from the joint space into the space of Cartesian displacement [9].

Specifically, taking an 2D case as an example, in the joint space, based on the torque limits, the left polytope in Fig.7 is available and after the transformation based on (6), we can plot the right polytope in Fig.7, which represents for the displacement of the e-e in the operational space [10]. As we

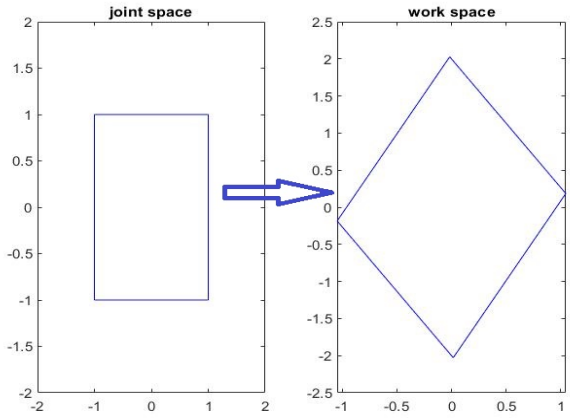

Fig. 7. SFP calculation

can see in the figure, the size for the polytopes are different. This is due to the jacobi matrix. In this function, the jacobi matrix not only maps the polytope from the joint space into the operational space, but also works like a gain, so that, the size of the polytope may change. Based on this method, we finally calculate the corresponding SFP(stiffness feasibility polytope).

Algorithm 2 GET SFP

input: Joint variable, $\underline{q}$;

1: Calculate the gravity torque, $\underline{\tau_g}$;

2: $\underline{F} \leftarrow (\underline{J(q)}^T)^{-1}[\underline{Rect_\tau} - \underline{\tau_g}]$;

▷ $\underline{J(q)}$ is a jacobian matrix.

▷ Vertexs of a polytope of joint torques, $\underline{Rect_\tau}$;

3: $SFP \leftarrow (\underline{K_c})^{-1}\underline{F}$;

In conclusion, the displacement range of the e-e is a regular polytope as illustrated in Fig.6 in red wth the torque limits. Then through rotation-scaling-rotation transformation the mulitidimensional regular polytope space is transformed into a mulitidimensional polytope [11].

The SFE(stiffness feasibility ellipsoid) region is always a part of SFP region for a manipulator with given actuators, which is illustrated in Fig.6 in red. However, SFP gives a more accurate description of the output capacity space than SFE. However, SFE is a fast and intuitive tool that conveys some information on the space of maximum allowable deviation from the initial equilibrium point of a compliant robot [12] [13].

The method to calculate SFE is shown as below, here the torque limits are taken into consideration.

$$\underline{\hat{\tau}} = \underline{W_\tau \tau} \tag{8}$$

where $\underline{W_\tau} = diag[\frac{1}{\tau_{lim_1}} \frac{1}{\tau_{lim_2}} \cdots \frac{1}{\tau_{lim_n}}]$, and τ_{lim_i} denote the torque limit of the joint number i ,that is, $|\tau_i| \leq \tau_{lim_i}$. The SFE is defined as

$$\underline{\delta x}||\underline{\hat{\tau}}|_2 \leq 1 \tag{9}$$

with$||_2$, denoting the two norm. It indicates the maximum allowable displacement for e-e under the limitations of the joint torques. Based on (8) and (9), we can calculate (8)

$$\underline{W_\tau \tau} \leq 1 \tag{10}$$

then we calculate

$$\underline{W_\tau J^T K_p \delta x} \leq 1 \tag{11}$$

$$\underline{\delta x} \leq (\underline{W_\tau J^T K_p})^{-1} \tag{12}$$

the equation(12) displays the maximun allowable boundary of e-e displacement fully. The set of orthonormal outputs of the SVD of $\underline{W_\tau J^T K_p}$ indicate the direction of the principal axes of the SFE, with the magnitudes calculated by the reciprocal of the corresponding eigenvalues.

Algorithm 3 GET SFE

input: Joint variable, $\underline{q}$;

1: $[u,s,v^T] \leftarrow SVD(\underline{W_\tau J(q)}^T \underline{K_c})^{-1}$;

▷ $\underline{K_c}$ is a stiffness matrix.

▷ $\underline{J(q)}$ is a jacobian matrix.

▷ $\underline{W_\tau}$ is a diagonal Matrix containing $\frac{1}{\tau_{limit}}$.

2: $[u',s',v'^T] \leftarrow$ choose columns of u, v^T corresponding to non-zero singular values;

3: $SFE \leftarrow u' s' v'^T$ unit circle;

In conclusion, results prove that even though both configurations achieve a similar endpoint stiffnessmatrix, their capabilities to confront external force/displacement differ.

III. OPTIMIZE SFE – REDUNDANT CASE

Due to the complexity of the SFR and SFP calculations for real-time applications, we compute the SFE by transforming the unit sphere in joint torque space into the task space and calculate its intersection with the image of the Jacobian transpose.

As mentioned earlier, stiffness feasibility ellipsoid is a fast and intuitive tool that conveys some information on the space of maximum allowable deviation from the initial equilibrium point of a compliant robot. Especially, the directions of the maximum/minimum allowable displacement and the isotropy index (ratio between the maximum and the minimum axis) of the ellipsoid are profitable properties which can provide insight into the role of robot configuration in Cartesian stiffness control capabilities. For instance, if the maximum axis of the realized SFE is elongated towards the direction of the external disturbance, the robot's Cartesian stiffness controller will be able to encounter larger deformation/force profiles prior to the occurrence of actuation torque saturation.

Our objective in this section is to explore algorithm to adjust robot redundancy to maximally align the direction of the maximum axis of the SFE with the external disturbance. Next, we explore the role of robot configuration to weaken the effect of gravity on the SFE's spatial translation. We take a 4 arms robot in two different configurations as an example. We treat this problem as optimization problem, so we need to determine cost function and constraints.

A. Optimize the SFR geometry

The length of the vector from the origin to the surface of the ellipsoid in the direction of $\frac{\delta x}{\|\delta x\|}$ specifies the maximum allowable e-e displacement prior to the actuation saturation. To compute this vector(σ), we can write

$$(\underline{W_\tau J}^T \underline{K_p} \sigma \frac{\delta x}{\|\underline{\delta x}\|})^T (\underline{W_\tau J}^T \underline{K_p} \sigma \frac{\delta x}{\|\underline{\delta x}\|}) = 1 \quad (13)$$

Solving for σ, we obtain

$$V_1 = \sigma = (\frac{\delta x^T}{\|\underline{\delta x}\|} \underline{K_p J W_\tau}^2 \underline{J}^T \underline{K_p} \frac{\delta x}{\|\underline{\delta x}\|})^{-0.5} \quad (14)$$

This σ equation is our cost function, we hope σ could be as large as possible in a given direction.

Then, in this example, the non-linear constraint is the e-e position should be fixed, which means the x-y coordinate of e-e is fixed. Here, we don't fix the orientation, because we only have 4DOF and we also want to do the optimization. By the command "fmincon" in matlab, we get optimized results.

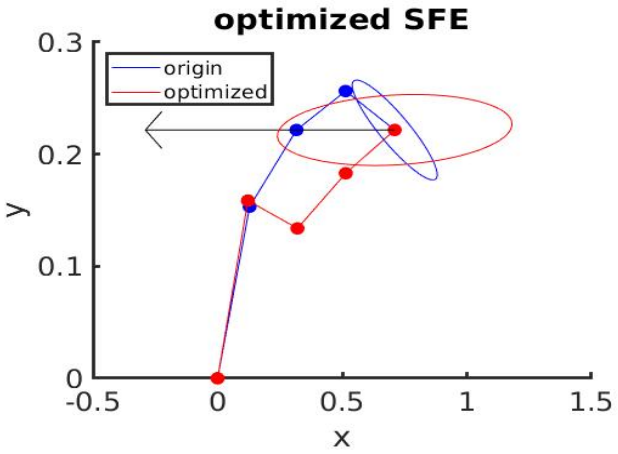

Fig. 8. Optimized SFE

In the Fig.8, we can see that after optimization, the length along the certain direction is increased. The right figure shows corresponding SFR and SFE. Optimized SFR also has larger length along the certain direction.

B. Minimizie the gravity effect on the SFR translation and geometry

A similar technique can be used to reduce the effect of gravity on the translation of the achieved SFE in the task space. We define the cost function

$$V_2 = \triangle x_g^T \triangle x_g \quad (15)$$

with $\triangle x_g = K_p^{-1} G_q$ and $G_q = (J^T)^{-1} \tau_g$. Iterative minimization of V will contribute to the reduction of the spatial translation of the SFE and the SFR, as a consequence. The result is shown in Fig.9.

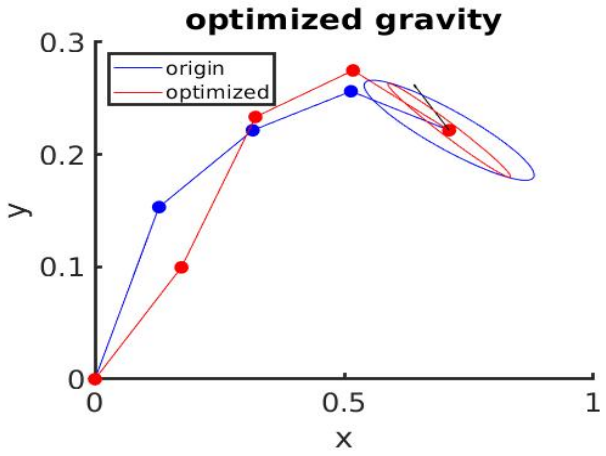

Fig. 9. The left figure compares SFE of original configuration with that of optimized configuration.

C. Combined Optimization

When considering to optimize SFE and minimize gravity effect at the same time, We modify our cost function

$$V = weightingfactor_1 * V_1 + weightingfactor_2 * V_2 \quad (16)$$

When we choose to be more care about minimizing gravity effect, the result is shown in Fig.10. If we compare Fig.10

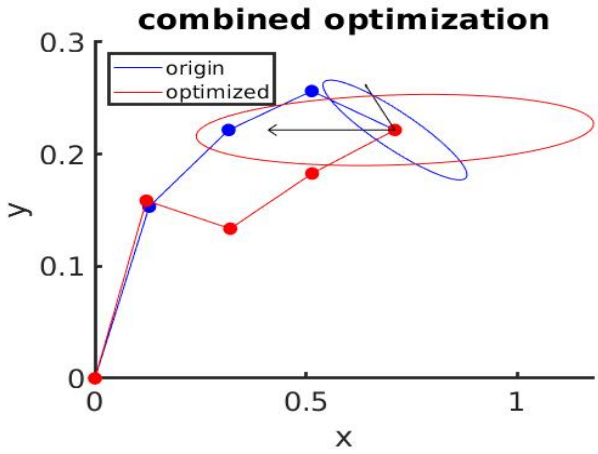

Fig. 10. Combined Optimization

with Fig.9 and Fig.8, we can find the robot configuration and SFE shape are different, so it works.

IV. CONCLUSIONS

In this paper, we research how large the area that the robot could maintain stiffness is, under the practical torque limitations and gravity effect. So that we introduce the concept of SFR and explain the role of configuration or pose of robot arm. Then to simplify calculation, SPE, SFP are also introduced. If the robot arm has redundancy, we could treat the problem that which configuration is the best for maintaining stiffness as a optimization problem. We also try minimizing the gravity effect for deviation of SFR, and combining both cost functions together.

REFERENCES

[1] Albu-Schaffer, Alin, et al. "Cartesian impedance control of redundant robots: Recent results with the DLR-light-weight-arms." 2003 IEEE International Conference on Robotics and Automation (Cat. No. 03CH37422). Vol. 3. IEEE, 2003.

[2] Pashkevich, Anatol, Alexandr Klimchik, and Damien Chablat. "Enhanced stiffness modeling of manipulators with passive joints." Mechanism and machine theory 46.5 (2011): 662-679.

[3] Huang, Chintien, and Imin Kao. "Geometrical interpretation of the cct stiffness mapping for serial manipulators." Robotics Research. Springer, Berlin, Heidelberg, 2003. 419-431.

[4] Mussa-Ivaldi, Ferdinando A., Neville Hogan, and Emilio Bizzi. "Neural, mechanical, and geometric factors subserving arm posture in humans." Journal of Neuroscience 5.10 (1985): 2732-2743.

[5] Burdet, E., et al. "A method for measuring endpoint stiffness during multi-joint arm movements." Journal of biomechanics 33.12 (2000): 1705-1709.

[6] Gribble, Paul L., et al. "Role of cocontraction in arm movement accuracy." Journal of neurophysiology 89.5 (2003): 2396-2405.

[7] Laursen, Bjarne, Bente Rona Jensen, and G. Sjgaard. "Effect of speed and precision demands on human shoulder muscle electromyography during a repetitive task." European Journal of Applied Physiology and Occupational Physiology 78.6 (1998): 544-548.

[8] Chiacchio, P., et al. "Influence of gravity on the manipulability ellipsoid for robot arms." Journal of Dynamic Systems, Measurement, and Control 114.4 (1992): 723-727.

[9] Nokleby, S. B., et al. "Force capabilities of redundantly-actuated parallel manipulators." Mechanism and machine theory 40.5 (2005): 578-599.

[10] Wei, Baochen, and Feng Gao. "A method to calculate working capacity space of multi-DOF manipulator and the application in excavating mechanism." Frontiers of Mechanical Engineering 7.2 (2012): 109-119.

[11] Ferreira, NM Fonseca, and JA Tenreiro Machado. "Manipulability analysis of two-arm robotic systems." Proc. of IEEE International Conference on Intelligent Engineering Systems. Vol. 1. No. 1. 2000.

[12] Yoshikawa, Tsuneo. "Manipulability of robotic mechanisms." The international journal of Robotics Research 4.2 (1985): 3-9.

[13] Chiacchio, Pasquale, Yann Bouffard?Vercelli, and Franois Pierrot. "Force polytope and force ellipsoid for redundant manipulators." Journal of Robotic Systems 14.8 (1997): 613-620.